Comprehensive current amplitude ratio based pilot protection for line with converter-interfaced sources

Yang, Zhe; Liao, Wenlong; Bak, Claus Leth; Chen, Zhe

Published in:
Energy Reports

DOI (link to publication from Publisher):
10.1016/j.egyr.2022.05.170

Publication date:
2022

Document Version
Publisher's PDF, also known as Version of record

Available online at www.sciencedirect.com
ScienceDirect
Energy Reports 8 (2022) 420–430
www.elsevier.com/locate/egyr

2022 The 4th International Conference on Clean Energy and Electrical Systems (CEES 2022), 2–4 April, 2022, Tokyo, Japan

Comprehensive current amplitude ratio based pilot protection for line with converter-interfaced sources

Zhe Yang, Wenlong Liao*, Claus Leth Bak, Zhe Chen

AAU Energy, Aalborg University, Aalborg, 9220, Denmark

Received 8 May 2022; accepted 18 May 2022
Available online xxxx

Abstract

Fault behaviours of converter-interfaced renewable energy sources (CIRESs) are greatly diverse from those of synchronous generators (SGs), so the traditional proportional restraint differential protection may fail to be activated. In order to deal with this issue, a comprehensive current amplitude ratio-based pilot relay is proposed. Since the fault current from CIRESs is much smaller than that of SGs, so phase current amplitude ratio on both end is lower than 1. In order to improve protection sensitivity for high resistance faults and grounding faults, sequence current ratio is also introduced to constitute a comprehensive protection criterion. The proposed method only uses the amplitude feature, so it has a lower time synchronization requirement for the currents on both terminals. Meanwhile, it can be applied for different fault ride through (FRT) strategies because the current limiting is always satisfied. Furthermore, the proposed method is easy to be deployed in protection devices after a small revision is done for the original protection algorithm. PSCAD simulation demonstrates that the proposed method is effective for different fault scenarios.

Peer-review under responsibility of the scientific committee of the 4th International Conference on Clean Energy and Electrical Systems, CEES, 2022.

Keywords: Current ratio; Comprehensive criterion; Converter-interfaced renewable energy sources; Pilot protection

1. Introduction

Renewable energy sources (RESs) have become an important part of modern power systems due to the low-carbon and sustainability [1,2]. Many European countries such as Denmark have declared that all the electric power will be from RESs by 2050 [3]. Different from synchronous generators (SGs), converter-interfaced RESs (CIRESs) are integrated into the grid through full-power inverters [4,5], so their distinctive fault signatures will threaten the correct operation of power system protection [6].

Pilot relay is often deployed on the transmission system because of absolute selectivity and short response time [7]. Among numerous pilot protection methods, the most frequently used is proportional restraint type

* Corresponding author.
E-mail address: weli@energy.aau.dk (W. Liao).

https://doi.org/10.1016/j.egyr.2022.05.170

Peer-review under responsibility of the scientific committee of the 4th International Conference on Clean Energy and Electrical Systems, CEES, 2022.

differential protection [8]. However, the fault current angle of CIRESs depends on current command values, but the related angle for SGs relies on the sequence impedance and the internal potential [9]. As a result, a big phase angle difference on both terminals may be present in some control strategies, which will result in the misoperation of differential relays [10]. In addition, when the integrated capacity of RESs is small, the operating current is close to the restraint current, so the sensitivity of the differential protection is relatively low [11]. In addition, directional elements on both terminals can communicate with each other to constitute a directional pilot protection [12]. A salient advantage for this protection is that it has minimum bandwidth requirements since only logic signals are transmitted [13]. However, the impedance angle of CIRESs may be far offset from 90° in some cases, so directional pilot protection faces adaptive problems [14]. Another pilot protection is called pilot distance protection that is constructed by two sides of distance relays with the communication system [15], but distance relays are vulnerable to fault resistance due to the weak infeed of CIRESs, so the pilot distance protection is also affected [16].

In order to cope with this issue, some new pilot protection methods have been put forward. The concept of differential impedance was introduced in [17], and internal or external faults can be identified by the difference in the impedance amplitude, but this scheme had a high demand for data synchronization on both ends. With reference to proportional restraint differential protection, a new pilot protection was constructed in [18] by comparing the differential impedance and braking impedance, but its performance will be severely degraded even though small fault resistances are added. In addition, the above two methods also use voltage phasors, so voltage transducers must be installed. Researchers in [19] came up with a pilot protection on account of the current frequency difference, but it is only applicable for doubly-fed induction generators (DFIGs). Travelling-wave protection methods also attracted some attention in recently years, but it needs a high sampling rate [20,21]. Some scholars come up with time-domain differential protection methods. In [22], the relationship between the different current and the derivative of the different voltage was analysed by establishing the circuit equations for internal and external faults, and the correlation difference was utilized to identify internal faults, but it is susceptible to high-frequency harmonics. In addition, the transient current difference on both sides could be identified by Cosine similarity and Euclidean distance in [23,24], but all the sampling values within 10 ms or 20 ms need to be transmitted to the remote end. In order to reduce the requirements for communication, a phase current amplitude ratio-based pilot protection was proposed in [25] because the fault current from CIRESs is much smaller than that on the grid side. However, the method can be a bit low for high resistance faults and grounding faults, therefore, more work needs to be done.

A comprehensive current amplitude ratio-based pilot protection is proposed, and it has the following advantages: (1) the protection principle is simple and can be easy to be deployed in protection devices. (2) Sequence current ratios are introduced to enhance the protection sensitivity for high resistance faults and grounding faults. (3) The proposed method has a low command for communication and strict data synchronization is not necessary. Simulation results in PSCAD validate the proposed method.

2. The tested system with CIRESs

A 220 kV transmission line with a CIRES power plant is established in PSCAD, as depicted in Fig. 1. The length of the transmission line is 80 km, the capacity of the power plant is 500 MW, and the grid impedance is 0.3+j9.42 Ω.

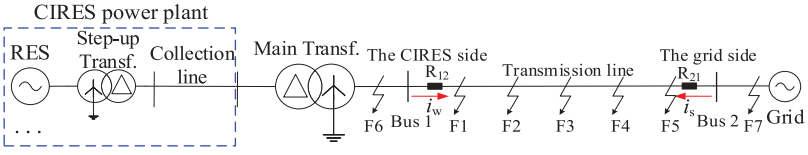

Fig. 1. The studied line topology with CIRESs.

In addition, the positive- and zero-sequence unit impedances of the transmission line are respectively 0.076+0.338 Ω and 0.284+0.824 Ω. Under this circumstance, the CIRES capacity is one-third of the short-circuit capacity of the grid measured at Bus 1. Pilot protection was installed at R_{12} and R_{21} to protect the entire transmission line. Four internal fault points are located at 0 km, 20 km, 40 km, 60 km and 80 km, which are respectively marked as F1, F2, F3, F4 and F5, and two external fault locations F6 and F7 are placed at left hand of Bus 1 and the right hand of Bus 2.

The grid-side controller based on decoupled sequence control is depicted in Fig. 2. The DC voltage is controlled to generate positive-sequence d-axis current reference on normal operation, and the negative-sequence current references are usually set to 0 [25]. The used voltage components and current components in the controller are measured at the right side and left side of the LCL filter. When a fault occurs, the outer voltage loop will be cut off, and positive-sequence current references will be set according to specific fault ride through (FRT) strategy in grid codes. In order to prevent the overvoltage on the DC side, a chopper circuit is installed.

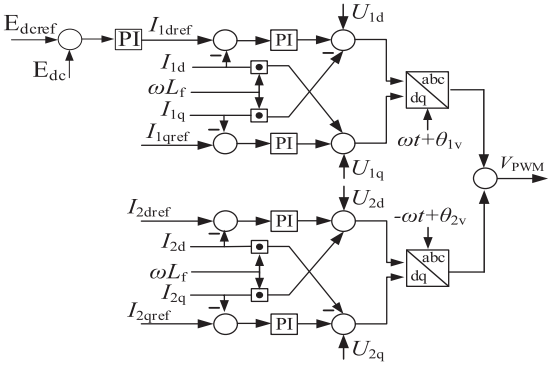

Fig. 2. The control diagram of CIRESs.

3. Problem statement

In this section, three common pilot protection methods will be analysed combined with typical FRT strategies.

3.1. Proportional restraint differential protection

Aimed at conventional transmission systems, the current angles on both terminals are the opposite on normal operation, but both are the same for in-of-zone faults, so the protection criterion of differential relays is [24]:

$$\begin{cases} I_{\mathrm{op}} \geq I_{\mathrm{op0}}, \text{ and } I_{\mathrm{op}} \geq kI_{\mathrm{res}} \\ I_{\mathrm{op}} = \left|\dot{I}_{\mathrm{S}} + \dot{I}_{\mathrm{W}}\right|, I_{\mathrm{res}} = \left|\dot{I}_{\mathrm{S}} - \dot{I}_{\mathrm{W}}\right| \end{cases} \tag{1}$$

where I_{res} denotes the restraint current, and I_{op} denotes the operating current. I_{op0} denotes the starting current, and k denotes the restraint coefficient that is set to 0.8 in this paper.

For SGs, the phase-A analytic expression for a three-phase fault is as follows [13]:

$$i_{\mathrm{SG}} = \sqrt{2}E_{\mathrm{q|0|}}/x_{\mathrm{d}} \cos(\omega_0 t + \varphi) - \frac{\sqrt{2}E_{\mathrm{q|0|}} \cos\varphi}{x_{\mathrm{d}}} \mathrm{e}^{-t/T_{\mathrm{a}}} \tag{2}$$

where $E_{\mathrm{q|0|}}$ denotes the induced voltage source, x_{d} is the synchronous reactance, and T_{a} is the decay time constant of the DC component. In addition, φ is the fault initial angle.

As shown in (2), the current angle is decided by sequence impedances and the induced voltage source before a fault, but the fault current angle of CIRESs depends on the specific control strategy, and its analytic expression is [26]:

$$i_{\mathrm{CIRES}} = \sqrt{I_{\mathrm{1dref}}^2 + I_{\mathrm{1qref}}^2} \cos\left(\omega t + \theta_{\mathrm{1v}} + \arctan\left(\frac{I_{\mathrm{1qref}}}{I_{\mathrm{1dref}}}\right)\right) \tag{3}$$

where ω denotes the synchronous angular velocity, and θ_{1v} denotes the phase-locked angle, and the maximum fault current is 1.2 p.u. in this paper.

It can be known from (3) that the fault current angle for CIRESs relies on the current references that are usually set according to the required FRT strategy. For this reason, the phase angle difference on both terminals might be very large in some cases. Therefore, proportional restraint differential protection faces huge challenges.

The FRT strategy about reactive current in Denmark is utilized to validate the performance of proportional restraint differential protection. With reference to the FRT strategy in Fig. 3, I_{1qref} is given according to the voltage drop. After that, I_{1dref} is calculated using the current limiting value and I_{1qref}. In addition, wind turbines must maintain the normal operation in Area A; In Area B, wind turbines must be connected to the grid within a fixed period of time, and they are allowed to be separated from the grid in Area C [27].

When CIRESs adopt the above the FRT strategy and a BC fault occurs at F1, the phase angle difference on both ends and operation results (I_{op} divided by I_{res}) of proportional restraint differential relays are illustrated in Fig. 3.

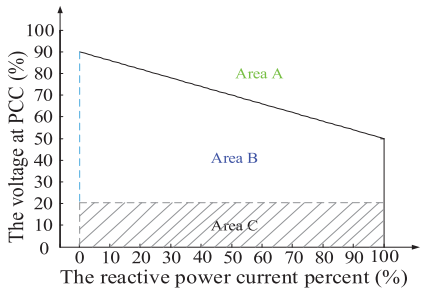

Fig. 3. FRT regulation in Denmark.

In Fig. 4(a), the phase angle differences for phase-B and phase-C are respectively 70.492° and 125.867°, so the phase-B ratio in Fig. 4(b) is higher than the threshold value, but the phase-C ratio is lower than the threshold value. Therefore, the phase-C differential protection will refuse to operate.

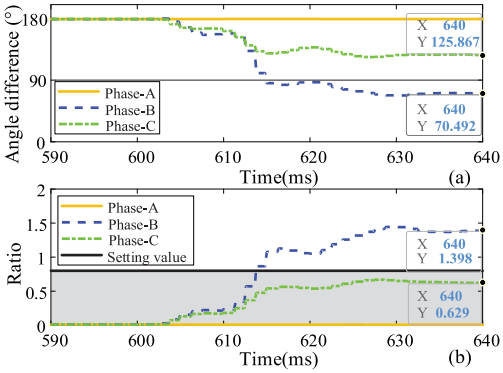

Fig. 4. The related measurements of differential relays for FRT in Denmark. (a) Angle difference, (b) operating results.

Another FRT strategy used in some North America utilities is that CIRESs do not inject reactive power into the grid during a fault. At this time, the angle differences on both sides and three-phase ratios for the proportional restraint differential protection are depicted in Fig. 5.

The angle differences of phase-B and phase-C in Fig. 5(a) are larger than 90°, so the ratios in Fig. 5(b) for phase-B and phase-C are respectively 0.758 and 0.508 that are smaller than the threshold value, so the differential protection will refuse to operate. Compared with the FRT strategy in Denmark, the control scheme without reactive power injection is more harmful to the correct operation of the differential protection.

3.2. Directional pilot protection

Directional relays play an important role in directional pilot protection. For the high-voltage transmission lines, the fault component based directional relays (FCBDRs) are often used including positive-sequence FCBDRs (PSFCBDRs), zero-sequence directional relays (ZSDRs) and negative-sequence directional relays (NSDRs). For a fault at the positive direction of the relay, the impedance angle measured by these directional relays should settle

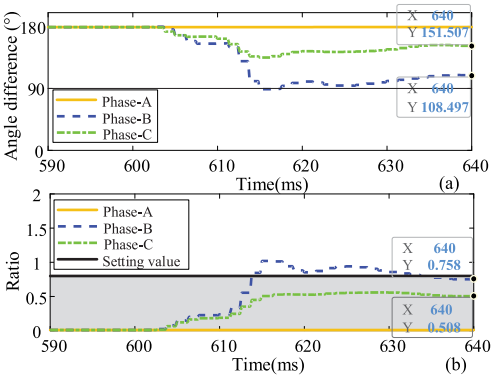

Fig. 5. The related measurements of differential relays for FRT in North America. (a) Angle difference, (b) operation results.

within between −180° and 0°. For a phase-A grounding at F2, the measured impedance angles are illustrated in Fig. 6 when FRT strategies in Denmark and North America are used.

The detected impedance angle for PSFCBDRs in Fig. 6(a) and is close to −180°, so this protection has a low sensitivity under Danish FRT strategy. In Fig. 6(b), it is equal to 66.891°, so the directional relay will misjudge the fault direction for the FRT scheme used in North American utilities. In addition, ZSDRs in Fig. 6(a) and (b) can operate correctly under two FRT strategies because the zero-sequence circuit is only composed of the part of the transmission line and the main transformer and does not include the equivalent impedance of CIRESs. For NSDRs, the negative-sequence current from CIRESs is always negligible, so the detected impedance angles for NSDRs in Fig. 6(a) and (b) will have a large oscillation, and NSDRs cannot detect the fault direction reliably.

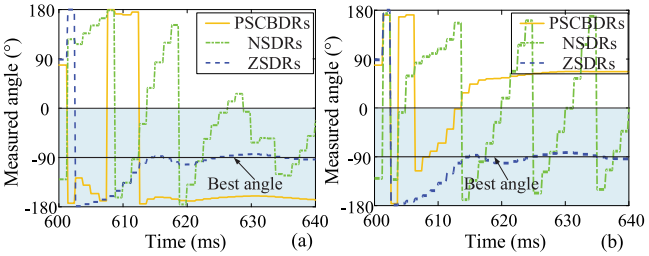

Fig. 6. Operation results of directional elements for two FRT schemes. (a) Denmark, (b) North America.

3.3. Pilot distance protection

The performance of pilot distance protection depends on that of distance relays. If a BC fault occurs at F3 with 10 Ω of fault resistance, the measured impedance trace is illustrated in Fig. 7 under two FRT strategies.

It can be known in Fig. 7 that the impedance traces are finally oriented at the third quadrant and the fourth quadrant for two different FRT control strategies, so distance protection will fail to operate, and pilot distance protection will also have adaptive problems.

4. Comprehensive current amplitude ratio based pilot protection

In this section, the fault current amplitude feature will be studied, and a comprehensive current amplitude ratio-based pilot protection will be put forward.

4.1. Protection principle

For a fault at the transmission line, the simplified circuit diagram is depicted in Fig. 8.

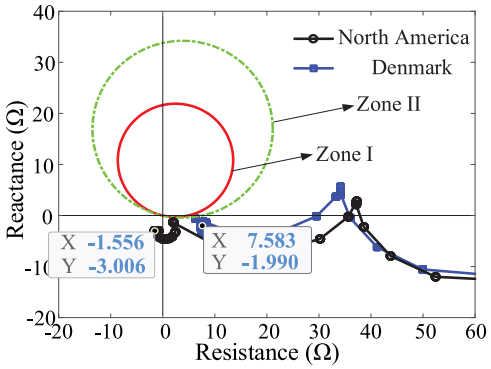

Fig. 7. Operation results of distance relays for two FRT schemes.

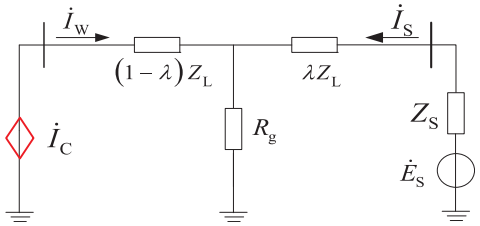

Fig. 8. The simplified fault equivalent circuit.

In Fig. 8, CIRESs are equivalent to a controllable current source, and the grid is equivalent to a voltage source with an impedance. Z_L is the entire line impedance, and λ is the ratio of the line impedance between the fault location and Bus 2 to the entire line impedance. R_g is the fault resistance. At this time, the currents on both ends should satisfy the following relationship:

$$\dot{I}_S\left(\lambda Z_L + Z_S\right) = \dot{E}_S - \left(\dot{I}_W + \dot{I}_S\right) R_g \tag{4}$$

Therefore, the current ratio ξ can be expressed as:

$$\xi = \left|\dot{I}_S/\dot{I}_W\right| = \left|\frac{\dot{E}_S/\dot{I}_W - R_g}{\lambda Z_L + Z_S + R_g}\right| \tag{5}$$

Since the maximum fault current from CIRESs is 1.2 p.u., the amplitude of $\dot{E}_S/\dot{I}_W$ is slightly smaller the load impedance, and much larger than R_g and (λZ_L+Z_S+R_g) when fault resistance is not too high. Therefore, the value of ξ is usually larger than 1. However, the fault current of CIRESs sometimes may be equal to 0 due to the lack of the light and wind, so the final protection criterion is as follows:

$$\eta_f = \left|\dot{I}_W/\dot{I}_S\right| < \eta_{set} \tag{6}$$

where η_{set} is the protection setting value.

However, the protection sensitivity is relatively low for high resistance faults and grounding faults, so positive- and negative-sequence current amplitude ratios are also introduced to enhance the protection sensitivity, so the comprehensive amplitude ratio can be expressed as:

$$\begin{cases} \eta_f = \left|\dot{I}_W/\dot{I}_S\right| < \eta_{set}, \eta_1 = \left|\dot{I}_{W1}/\dot{I}_{S1}\right| < \eta_{set} \\ \eta_2 = \left|\dot{I}_{W2}/\dot{I}_{S2}\right| < \eta_{set} \end{cases} \tag{7}$$

where subscripts 1 and 2 denote the corresponding positive- and negative-sequence components.

When one of η_f, η_1, and η_2 is satisfied, the protection is activated to trip the line. The setting principle will be detailed in the next section.

4.2. Protection setting

For the SG current in (2), it will contain the attenuated DC component in the transient process, which will lead to a small error to extraction of power frequency components, so its impact needs to be considered in the protection setting. In addition, the current transducers (CTs) on both ends may have a difference in both types and measurement accuracy. When these factors are considered, the setting value is:

$$\eta_{set} = 1 - \rho_{rel}\rho_{er}\rho_{st}\rho_{np} \tag{8}$$

where ρ_{rel} denotes the reliability factor that is usually from 1.2 to 1.3. ρ_{er} denotes the error coefficient of the CT that is usually is set to 1.1. ρ_{st} denotes the CT same type coefficient. When CTs on both ends belong to the same type, ρ_{st} is 0.5, and it will be taken as 1 when they are different. ρ_{np} denotes non-periodic component coefficient. It is set to 1 when a fast saturation relay is adopted, and if there is a series resistance to eliminate the unbalanced current, ρ_{np} can be chosen between 1.5 and 2 [28]. According to the above content, η_{set} can be taken as 0.82. Since the impact of the DC component and CTs on phase currents and sequence currents is basically same, so the setting value is unified for η_f, η_1, and η_2.

The proposed protection does not have the phase selection function when sequence current ratio is used, so it needs an extra phase selector because the single-phase tripping is required for the transmission system. In addition, the fault starting element should be also used. The specific flowchart is depicted in Fig. 9.

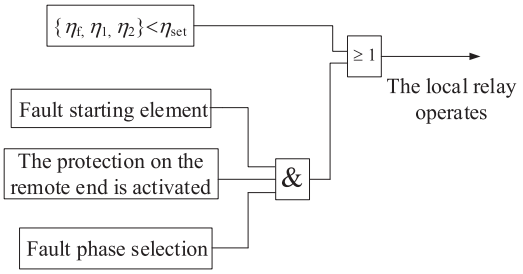

Fig. 9. The detailed flowchart.

5. Simulation analysis

Simulation analysis will be done considering the impact of different factors. CIRESs always operates at the unity power factor on normal operation, and the FRT strategy in Denmark will be used during a fault at 600 ms.

5.1. Different fault points and fault types

First, the simulation results about phase current ratio for internal faults at F1 are depicted in Fig. 10. The proposed approach can detect this internal fault in Fig. 10(b) for the same fault conditions. For AG faults and ABC faults Fig. 10(a) and (d), η_f for faulty phases is always smaller than the threshold value, which proves that this new protection can operate correctly. However, the phase-C sensitivity is very low for BCG fault in Fig. 10(c) because there will be a large zero-sequence current on the CIRES end at this time. Therefore, positive- and negative-sequence current amplitude ratios is necessary to enhance the protection sensitivity, as shown in Fig. 11.

The curve with the lowest sensitivity between faulty phases in Fig. 10 is taken as η_f in Fig. 11 because the worst case needs to be considered in the protection field. For AG faults and BC faults in Fig. 11(a) and (b), η_1 is the highest, and η_2 is the smallest due to no negative-sequence current from CIRESs, so the criterion based on negative-sequence current amplitude ratio has the highest sensitivity. In addition, η_f is larger than η_1 in Fig. 11(c), so the method based positive-sequence current ratio has higher sensitivity for BCG faults. For ABCG faults in Fig. 11(d), η_1 is basically equal to η_f because the fault currents only include the positive-sequence currents on both ends, and the curve η_2 is meaningless at this time. Similarly, η_2 before the fault time in Fig. 11 is also meaningless, so the criterion based on negative-sequence current ratio should be activated after the fault are identified.

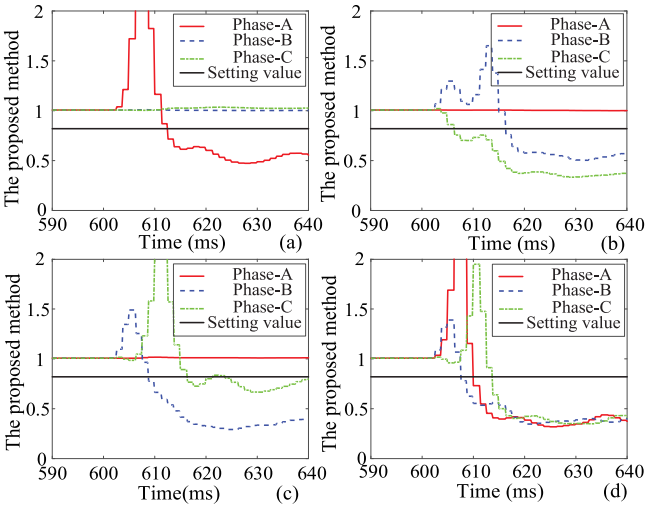

Fig. 10. The performance of the phase current ratio for internal faults. (a) AG faults, (b) BC faults, (c) BCG faults, (c) ABCG faults.

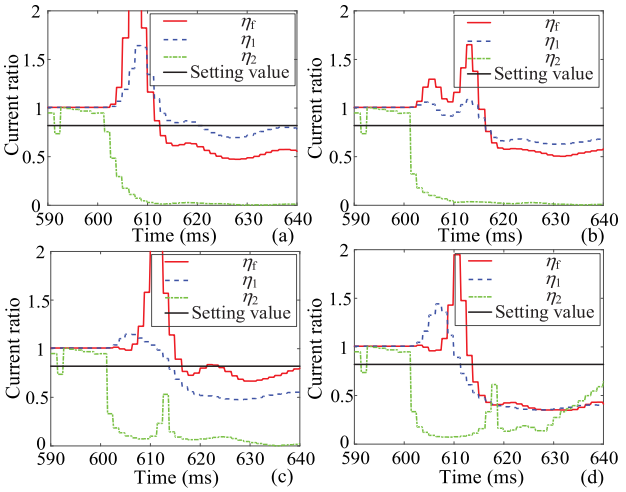

Fig. 11. The performance of the comprehensive ratio for internal faults. (a) AG faults, (b) BC faults, (c) BCG faults, (c) ABCG faults.

In addition, Fig. 12 depicts the measurements of this new protection for external failures at F6. Since the curves for four kinds of fault types are similar, so only the performance for AG faults and BC faults is given.

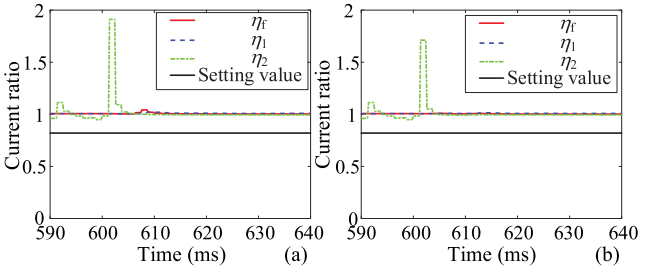

Fig. 12. The performance of the comprehensive criteria for external faults. (a) AG faults, (b) BC faults.

It can be seen from Fig. 12 that η_f, η_1 and η_2 are close to 1 at 640 ms and higher than the setting value for AG faults and BC faults, so the comprehensive criteria can be blocked reliably.

5.2. Faults with different fault resistances

In this part, the impact of fault resistance will be considered. Since the fault current on the grid side is the smallest when a fault appears at the exit of R_{12}, the ability to resist fault resistance is also weakest at this time. Therefore, the simulation results for different fault resistances are given in Table 1 for faults at F1. Since the fault resistance is usually smaller than 20 Ω for BC faults, the maximum value is set to 20 Ω. In addition, the maximum fault resistance for grounding faults is taken as 100 Ω. All the values in Table from the data at 640 ms.

In Table 1, η_2 is much smaller than the setting value for asymmetric faults, so this new protection can be activated to trip the line even for high resistance faults. However, the comprehensive criterion can only withstand 25 Ω of fault resistance for ABCG faults, so more effective methods can be studied for this fault scenario.

Table 1. Amplitude ratio under different fault resistances.

Fault type	Fault resistance (Ω)	η_f	η_1	η_2
AG	10	1.210	1.210	0.010
	25	1.740	1.597	0.010
	50	2.728	1.495	0.002
	100	2.766	1.379	0.002
BC	5	0.720	0.844	0.002
	10	0.740	0.907	0.002
	15	0.761	0.976	0.002
	20	0.787	1.050	0.002
BCG	10	1.473	0.749	0.001
	25	1.532	1.198	0
	50	2.041	3.610	0.002
	100	2.350	2.314	0.004
ABCG	10	0.476	0.475	/
	25	0.606	0.605	/
	50	1.411	1.408	/
	100	7.692	7.650	/

5.3. Faults with different FRT strategies

The impact of FRT strategies must be analysed in this part. Besides FRT strategies in Denmark and North America, another two will also be analysed. For the controller based on sequence control, the control objective of suppressing active power fluctuation or suppressing reactive power fluctuation can be achieved [14]. The performance of the comprehensive ratio under four control strategies is given in Fig. 13 when a BC fault appears at F3. For suppressing active power oscillation, the average active and reactive power references P_0 and Q_0 are respectively equal to 0.5 p.u. and 0.2 p.u., and the power references are the same for suppressing reactive power oscillation.

η_2 in Fig. 13(a) and (b) is the smallest and close to 0 because negative-sequence current references are usually set to 0 under FRT schemes in Denmark and North America. Additionally, η_2 is no longer equal to 0 for suppressing active and reactive power fluctuation in Fig. 13(c) and (d), but is still the smallest. Since η_2 is always lower than the threshold value, the comprehensive criterion is effective for different FRT strategies.

6. Conclusion

The controlled current angle of CIRESs can bring about the misoperation of the conventional proportional restraint differential protection, and the simulation results validate this conclusion combined with different FRT strategies.

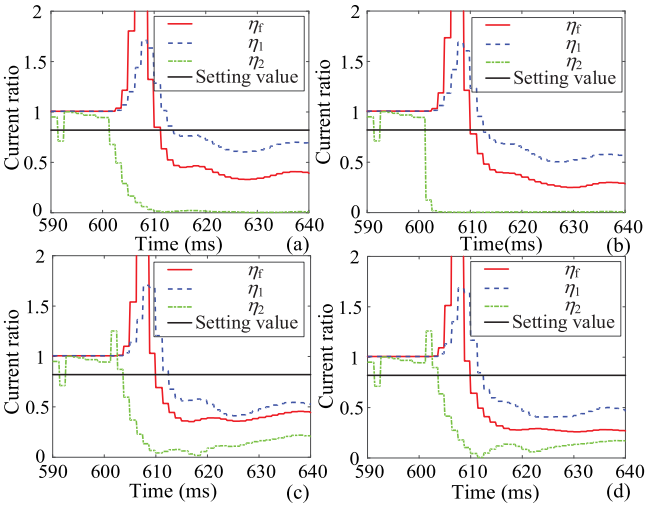

Fig. 13. The performance of the proposed method for diverse FRT schemes. (a) Denmark, (b) North America, (c) eliminating active power oscillation, (c) eliminating reactive power oscillation.

So as to cope with this issue, a comprehensive current amplitude ratio-based pilot protection is put forward. Since the CIRES fault current is much smaller than that on the grid side, the current amplitude ratio on both ends will be smaller than 1. For protection sensitivity for high resistance faults and grounding faults, sequence current ratio is also utilized to form a comprehensive criterion. The proposed approach only uses amplitude feature, so the strict time synchronization is not necessary. In addition, it is easy to be deployed in the protection devices because fast Fourier algorithm is still being used. Furthermore, it is also applicable for the scenario that CIRESs have no output power. PSCAD simulation results confirm the effectiveness and reliability of the proposed scheme.

Declaration of competing interest

The authors declare that they have no known competing financial interests or personal relationships that could have appeared to influence the work reported in this paper.

Acknowledgements

This work was supported by the China Scholarship Council (CSC) and AAU Ph.D. tuition fee scholarship.

References

[1] Mai T, et al. Renewable electricity futures for the United States. IEEE Trans. Sustain. Energy 2014;5(2):372–8.
[2] Zhuang YP, Liang H, Pomphrey M. Stochastic multi-timescale energy management of greenhouses with renewable energy sources. IEEE Trans. Sustain. Energy 2019;10(2):905–17.
[3] Jia J, Yang G, Nielsen AH. A review on grid-connected converter control for short-circuit power provision under grid unbalanced faults. IEEE Trans Power Del 2018;33(2):649–61.
[4] Ahmad T, et al. Field implementation and trial of coordinated control of WIND farms. IEEE Trans Sustain Energy 2018;9(3):1169–76.
[5] Firouzi M, Gharehpetian GB, Mozafari B. Power-flow control and short-circuit current limitation of wind farms using unified interphase power controller. IEEE Trans Power Del 2017;32(1):62–71.
[6] Telukunta V, Pradhan J, Agrawal A, Singh M, Srivani SG. Protection challenges under bulk penetration of renewable energy resources in power systems: A review. CSEE J Power Energy Syst 2017;3(4):365–79.
[7] Liu S, Zhang LL, Fu C, Jiang L. A new two-port network model-based pilot protection for AC transmission lines. IEEE Trans Power Del 2020;35(2):473–82.
[8] Ashrafian A, Mirsalim M, Masoum MAS. Application of a recursive phasor estimation method for adaptive fault component based differential protection of power transformers. IEEE Trans Ind Informat 2017;13(3):1381–92.
[9] Hooshyar A, Azzouz MA, El-Saadany EF. Distance protection of lines connected to induction generator-based wind farms during balanced faults. IEEE Trans Sustain Energy 2014;5(4):1193–203.
[10] Jia K, Yang Z, Zheng L, Zhu Z, Bi T. Spearman correlation-based pilot protection for transmission line connected to PMSGs and DFIGs. IEEE Trans Sustain Energy 2021;17(7):4532–44.

[11] Dambhare S, Soman SA, Chandorkar MC. Adaptive current differential protection schemes for transmission-line protection. IEEE Trans Power Del 2009;24(4):1832–41.
[12] Zou G, Gao H, Tong B, Zhu G, Zhao B. Directional pilot protection method for distribution grid with DG. In: 12th IET international conference on developments in power system protection. 2014, p. 1–5.
[13] Hooshyar A, Azzouz MA, El-Saadany EF. Distance protection of lines connected to induction generator-based wind farms during balanced faults. IEEE Trans Sustain Energy 2014;5(4):1193–203.
[14] Jia K, Yang Z, Fang Y, Bi T, Sumner M. Fluence of inverter-interfaced renewable energy generators on directional relay and an improved scheme. IEEE Trans Power Electron 2019;34(12):11843–55.
[15] Zheng T, Zhao Y, Li J, Wei X, Wang Y, Wang Z. A new pilot distance protection scheme for teed lines. In: 12th IET international conference on ac and dc power transmission. 2016, p. 1–5.
[16] Fang Y, Jia K, Yang Z, Li Y, Bi T. Impact of inverter-interfaced renewable energy generators on distance protection and an improved scheme. IEEE Trans Ind Electron 2019;66(9):7078–88.
[17] Bolandi TG, Seyedi H, Hashemi SM, Nezhad PS. Impedance-differential protection: A new approach to transmission-line Pilot protection. IEEE Trans Power Del 2015;30(6):2510–8.
[18] Chen G, Liu Y, Yang Q. An impedance-based protection principle for active distribution network. In: 2018 china international conference on electricity distribution. CICED, Tianjin; 2018, p. 1241–5.
[19] Cao N, Ge T, Yu Q. Research on main transformer protection of doubly-fed wind farm based on fault current frequency difference. In: 2018 chinese automation congress. CAC, Xi'an, China; 2018, p. 4067–72.
[20] Tang L, Dong X, Shi S, Wang B. Travelling wave differential protection based on equivalent travelling wave. In: 13th international conference on development in power system protection 2016. 2016, p. 1–6.
[21] Costa FB, Monti A, Lopes FV, Silva KM, Jamborsalamati P, Sadu A. Two-terminal traveling-wave-based transmission-line protection. IEEE Trans Power Del 2017;32(3):1382–93.
[22] Kang Xiaoning, Suonan Jiale, Song Guobin, Bo ZQ. Protection technique based on parameter identification-its principle and application. In: 2008 IEEE power and energy society general meeting - conversion and delivery of electrical energy in the 21st century. Pittsburgh, PA; 2008, p. 1–6.
[23] Zheng L, Jia K, Bi T, Fang Y, Yang Z. Cosine similarity based line protection for large-scale wind farms. IEEE Trans Ind Electron 2021;68(7):5990–9.
[24] Yang Z, Liao W, Wang H, Bak CL, Chen Z. Improved Euclidean Distance Based Pilot Protection for Lines with Renewable Energy Sources.In IEEE Trans Sustain Energy.
[25] Jia K, et al. Amplitude comparison based pilot protection for renewable power teed line.In CSEE Journal of Power and Energy Systems.
[26] Banaiemoqadam A, Hooshyar A, Azzouz MA. A control-based solution for distance protection of lines connected to converter-interfaced sources during asymmetrical faults. IEEE Trans Power Del 2020;35(3):1455–66.
[27] Piya P, Ebrahimi M, Karimi-Ghartemani M, Khajehoddin SA. Fault ride-through capability of voltage-controlled inverters. IEEE Trans Ind Electron 2018;65(10):7933–43.
[28] Horowitz SH, Phadke AG. Power systems relaying. USA: Wiley: Research Study Press; 2008.